Nanoimaging of Open-Circuit Voltage in Photovoltaic Devices

*Elizabeth M. Tennyson, Joseph L. Garrett, Jesse A. Frantz, Jason D. Myers, Robel Y. Bekele, Jasbinder S. Sanghera, Jeremy N. Munday, and Marina S. Leite**

For most photovoltaic (PV) devices, the record short-circuit current density is near its theoretical limit; however, achieving a large open-circuit voltage has proven difficult for nearly all photovoltaic technologies.[1,2] Understanding the carrier recombination processes, caused by structural or compositional variations at the nanoscale, that lead to this voltage reduction is critical, yet no technique exists to quantitatively map recombination and the resulting open-circuit voltage (V_{oc}) at the nanoscale. Here, we present a novel metrology to image the V_{oc} with spatial resolution <100 nm, more than five orders of magnitude better than previous methods, using a variant of illuminated Kelvin probe force microscopy (KPFM). We apply this technique to several materials (GaAs, Si, CdTe, and CIGS), and find that the V_{oc} varies locally by more than 200 mV, suggesting that spatial variation of nonradiative recombination strongly affects the overall device performance. This technique enables new insights into the loss mechanisms that hinder solar cells and provides a new platform to image device performance with nanoscale resolution.

The V_{oc} of a solar cell is a measurement of the maximum voltage generated by the device under illumination, which is proportional to the quasi-Fermi level splitting of the semiconductor p-n junction. The V_{oc} is a key figure of merit to define how well any PV device operates. This generated voltage and the overall electrical behavior of a device strongly depend on the nonradiative recombination rate of the charge carriers within a material, which is affected by the defects inherently present within the semiconductor. Despite all the efforts in developing higher performance thin-film polycrystalline solar cells, such as CdTe, $CuIn_xGa_{(1-x)}Se_2$ (CIGS), and Cu_2ZnSnS_4 (CZTS), the difference between the theoretically predicted and the best experimentally achieved V_{oc} is still considerably large (up to 0.6 V).[2,3] For Si, extensive research has been dedicated to design and implement nanostructured light-trapping architectures to boost light absorption;[4–7] however, there are very few experiments showing how the V_{oc} is affected. For organic PV blends, the limited V_{oc} observed in most bulk heterojunction solar cells is attributed to geminate and nongeminate losses;[8,9] nevertheless, local variations in V_{oc} have never been measured. Thus, for any micrometer- and nanoscale structured PV device, assessing variations in V_{oc} with nanoscale resolution and spatially resolving where recombination occurs within the material can potentially change the pathway for designing higher performance devices.

Imaging methods based on atomic force microscopy (AFM) techniques have been extensively used to characterize the structural and electrical properties of PV materials and full devices.[10–21] In particular, Kelvin probe force microscopy (KPFM) has been implemented to probe the electrical characteristics of a variety of PV materials and devices, ranging from organic materials[9,22–24] and oxides[25] to III–V semiconductors for multijunction designs[26–28] and polycrystalline thin films.[18,29–35] The local optoelectronic properties and changes in material composition have also been mapped using near-field scanning optical microscopy (NSOM) probes as local sources of excitation.[36–42] Very recently, photoluminescence has emerged as a promising tool to map charge recombination[43–45] and carriers diffusion[46] with high spatial resolution. At low temperature (70 K), photoluminescence imaging with submicrometer resolution has been implemented to map a 10 meV quasi-Fermi level splitting in CIGS solar cells, where variations in the intensity signal were attributed to changes in the material composition.[47] Nevertheless, none of these imaging techniques provide a direct measurement of V_{oc} within the material at operating conditions. A straightforward, universal, and accurate method to measure the V_{oc} (and hence nonradiative recombination processes) with high spatial resolution in PV materials is still missing.

Here, we present a new imaging technique based on illuminated KPFM to map the V_{oc} of optoelectronic devices with nanoscale resolution <100 nm. We map the contact potential difference (CPD) of half or fully processed solar cells in the

E. M. Tennyson, Prof. M. S. Leite
Department of Materials Science and Engineering
University of Maryland
College Park, MD 20742, USA
E-mail: mleite@umd.edu

E. M. Tennyson, J. L. Garrett, Prof. J. N. Munday, Prof. M. S. Leite
Institute for Research in Electronics and Applied Physics
University of Maryland
College Park, MD 20742, USA

J. L. Garrett
Department of Physics
University of Maryland
College Park, MD 20742, USA

Dr. J. A. Frantz, Dr. J. D. Myers, Dr. J. S. Sanghera
U.S. Naval Research Laboratory
Washington, DC 20375, USA

R. Y. Bekele
University Research Foundation
Greenbelt, MD 20770, USA

Prof. J. N. Munday
Department of Electrical and Computer Engineering
University of Maryland
College Park, MD 20742, USA

DOI: 10.1002/aenm.201501142

© 2015 WILEY-VCH Verlag GmbH & Co. KGaA, Weinheim

dark and under illumination to determine the quasi-Fermi level splitting of the p-n junction. We spatially resolve the V_{oc} of different PV materials, including III–V direct band gap semiconductors, monocrystalline Si, and polycrystalline thin films, demonstrating the universality of our platform for imaging devices' performance. While single crystalline GaAs and Si solar cells show very uniform V_{oc} maps, CdTe and CIGS present dramatic variations in V_{oc}, larger than 0.2 V, which have never been resolved by other microscopy methods. We find that the local variations in the V_{oc} are due to the fact that different grain orientations can act as distinct centers for recombination within the material. Although KPFM measurements under illumination (named surface photovoltage—SPV) have been realized in a variety of solar cells technology,[48–59] we demonstrate for the first time the direct correlation between SPV measurements (light minus dark KPFM) and the V_{oc} of photovoltaic devices, through the measurement of the quasi-Fermi level splitting. Our nanoscale metrology is nondestructive and can be implemented in ambient conditions, allowing for the diagnosis of how the different processing steps can affect the recombination within the material and, therefore, the ultimate performance of an optoelectronic device. For nonuniform semiconductor materials, mapping local variations in V_{oc} is extremely useful to identify which types of interfaces can suppress nonradiative recombination processes.

We implement illuminated KPFM as a new tool to directly map the V_{oc} of photovoltaic materials with nanoscale resolution. In KPFM, the CPD is proportional to the work function difference between the tip and the surface of the material under investigation ($qV_{CPD} = W_{tip} - W_s$). For a solar cell, as shown in **Figure 1**a,b, the CPD signal depends on the illumination conditions as

$$q \cdot V_{CPD}^{d} = W_{tip}^{d} - W_{s}^{d} \quad \text{(in the dark)} \tag{1}$$

and

$$q \cdot V_{CPD}^{il} = W_{tip}^{il} - W_{s}^{il} = (q \cdot V_{CPD}^{d}) + \Delta\mu \quad \text{(under illumination)} \tag{2}$$

where q is the electron charge, the superscripted d and il refer to dark and illuminated conditions, respectively, and $\Delta\mu$ is the quasi-Fermi level splitting. The V_{oc} of the device is

$$V_{oc} = \frac{\Delta\mu}{q} = V_{CPD}^{il} - V_{CPD}^{d} \tag{3}$$

Note that our technique does not require the preceding knowledge of the work function of the sample or the tip, because $\Delta\mu$ is determined by measuring the difference between these two quantities under distinct illumination conditions. Thus, the nanoscale maps of the V_{oc} of partially processed devices are determined from a pair of dark and illuminated KPFM images.

We implement amplitude-modulated (AM) KPFM using metal-coated Pt probes with mechanical resonance $\omega/2\pi = 86.7$ kHz in ambient conditions—see schematic setup in Figure 1c. For each scan, the probe passes over the surface twice. On the first pass, a feedback loop controls the sample height in order to maintain constant cantilever oscillation amplitude, and topography is acquired in noncontact mode. On the second pass, the cantilever is held at a constant height (ΔH) relative to the path it traced on the first pass—see Figure 1c. The tip oscillates slightly below resonance during the topographic scan, to maintain stable tapping mode.[60] The amplitude of the tip oscillation is ≈60 nm (though this value varies slightly from scan to scan, depending on the optical lever sensitivity of the probe).

The V_{oc} of a photovoltaic device is given by

$$V_{oc} = \frac{nkT}{q}\ln\left(\frac{I_{il}}{I_{dark}} + 1\right) \cong \frac{nkT}{q}\ln\left(\frac{I_{il}}{I_{dark}}\right) \tag{4}$$

where n is the ideality factor, k is Boltzmann's constant, T is the temperature, and I_{il} and I_{dark} are the light generated and the

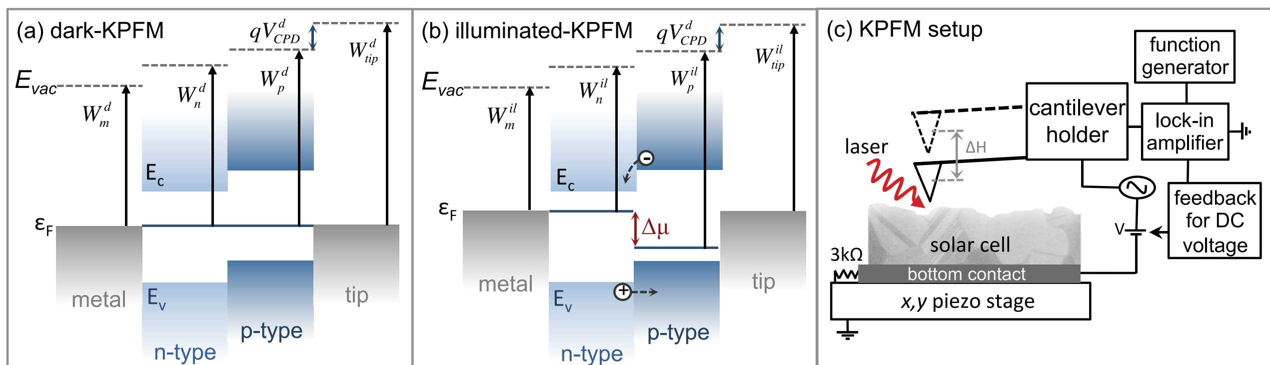

Figure 1. Band profile of n-p junction a) in equilibrium (dark) and b) under illumination. E_{vac}, E_c, E_v, and ε_F refer to the energy of the vacuum level, the conduction band, the valence band, and the Fermi level, respectively. $W_n^{d(il)}$ and $W_p^{d(il)}$ are the work function for the dark (illuminated) n- and p-type layers. E_{Fn} and E_{Fp} refer to the Fermi level splitting $\Delta\mu$ upon illumination. c) Cross-sectional illustration of illuminated KPFM setup, used to map V_{oc} of photovoltaic materials with nanoscale resolution. The metrology is implemented in ambient environment and only requires the bottom contact of the device. For each scan, the probe passes over the surface twice: in the first one topography is acquired, and in the second one the potential difference is recorded at a height ΔH from the first pass. The illumination source is a 660 nm continuum laser (represented by the red arrow). The SPV, difference between the illuminated and dark KPFM signals, is proportional to the V_{oc} of the solar cell.

© 2015 WILEY-VCH Verlag GmbH & Co. KGaA, Weinheim

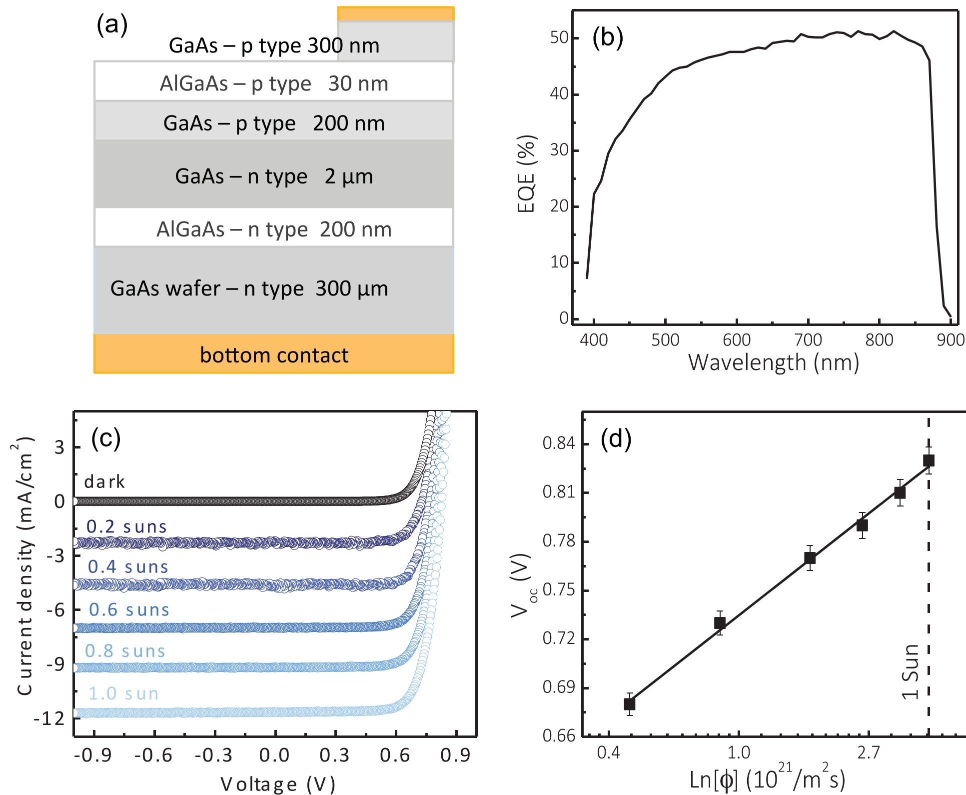

Figure 2. a) Schematic of the solar cell. b) External quantum efficiency measurement. c) Light *I–V* curves as a function of illumination (incident power). At AM 1.5G 1 sun illumination, $V_{oc} = 0.83 \pm 0.01$ V. d) Open-circuit voltage V_{oc} as a function of incident power (photon flux).

dark saturation current, respectively. For a partially illuminated solar cell the V_{oc} can be written as

$$V_{oc}^{partial}(\phi) = \frac{nkT}{q}\left\{\ln\left(\frac{q\cdot\phi\cdot EQE_o}{J_{dark}}\right) + \ln\left(\frac{\tau\cdot A_{il}\cdot EQE_{\lambda,\theta}}{A_{cell}\cdot EQE_o}\right)\right\} = V_{oc}^{full}(\phi) + \beta \quad (5)$$

where $I_{il} = q\cdot\phi\cdot EQE_{\lambda,\theta}\cdot A_{il}$, ϕ is the number of photons per area per time from the light source, EQE_o and $EQE_{\lambda,\theta}$ are the external quantum efficiencies at normal incidence and at an incident angle θ for illumination at wavelength λ, J_{dark} is the dark current density, τ is the transmission fraction of the optical setup, A_{il} is the area of the solar cell being illuminated, A_{cell} is the total area of the solar cell, and β is a calibration constant (<0), given by

$$\beta = \frac{nkT}{q}\left\{\ln\left(\frac{\tau\cdot A_{il}\cdot EQE_{\lambda,\theta}}{A_{cell}\cdot EQE_o}\right)\right\} \quad (6)$$

Note that for illumination of the full device, as is the case for a solar simulator measurement, $\beta = 0$.

With KPFM, the solar cells are only partially illuminated, and the light generated current is very small compared to the situation of full cell illumination. To determine the expected V_{oc} for full illumination using KPFM

$$V_{oc}^{full}(\phi) = V_{oc}^{partial}(\phi) - \beta \quad (7)$$

where $V_{oc}^{partial}(\phi)$ is the illuminated minus dark KPFM voltage signal, i.e., the SPV of the cell. Alternatively, if $V_{oc}^{full}(\phi)$ is determined by an independent method, e.g., from solar simulator measurements, for the same photon flux as the KPFM measurements, β can be experimentally determined as

$$\beta \cong V_{oc}^{partial}(\phi) - V_{oc}^{full}(\phi) \quad (8)$$

For our calibration of β, ϕ corresponds to 1 sun illumination (see Figure S2, Supporting Information).

Figure 2 shows the macroscopic characterization of a GaAs solar cell, without an antireflection coating, used to calibrate and test our new metrology; a schematic of the solar cell is presented in Figure 2a. Figure 2b shows the external quantum efficiency (EQE) measurement for the device under normal incidence illumination. The dark and light *I–V* macroscopic measurements were performed using a conventional solar simulator, where we adjust the light intensity to mimic different numbers of suns. The electrical characterization of the device shows good diode behavior, with $V_{oc} = 0.83 \pm 0.01$ V under 1 sun illumination (see Figure 2c). From the intensity-dependent light *I–V* curves we infer the V_{oc} dependence with illumination (see Figure 2d), where the photon flux corresponds to the Air Mass 1.5 global illumination, from 0.1 to 1.0 sun (100 mW cm^{-2}).

Figure 3 shows a sequence of intensity-dependent KPFM measurements. The GaAs solar cell is ideal to test our method because it is a very uniform sample (single crystal) with minimum height variation (roughness is 5 nm, see Figure 3a). The CPD (voltage signal) of the device increased with the incident

© 2015 WILEY-VCH Verlag GmbH & Co. KGaA, Weinheim

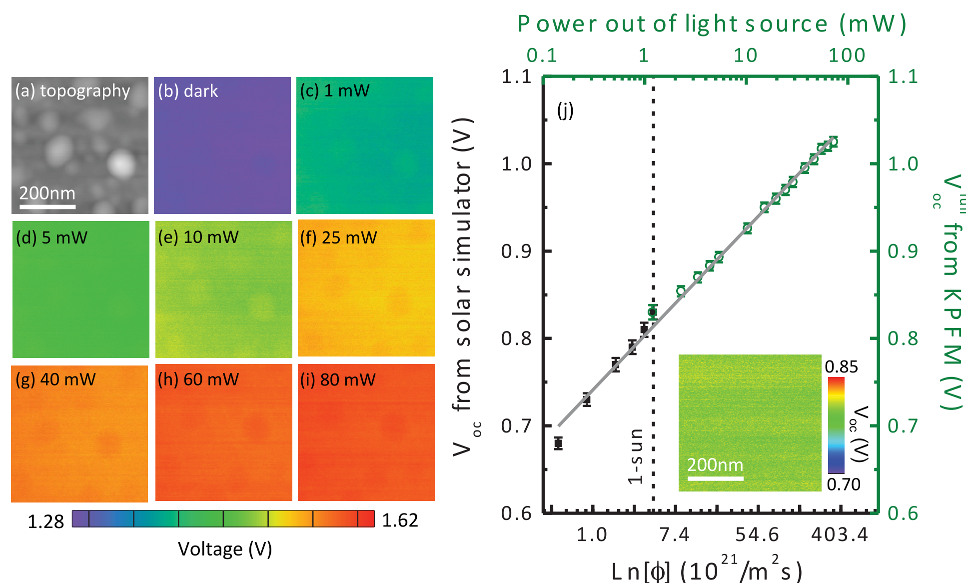

Figure 3. a) AFM topography image (peak to valley = 5 nm). b–i) KPFM images (V_{CPD}) for different incident powers (light source: 660 nm laser). j) V_{oc} determined by macroscopic *I–V* measurements (black) and by nanoscale KPFM (green) as a function of incident power from the light sources. For the KPFM measurements, the V_{oc} was obtained by averaging over the scanned area, and the error bars refer to the standard deviation. Inset shows uniform V_{oc} map with nanoscale resolution.

laser power (photon flux)—see Figure 3b–i—indicating that more carriers are generated upon increasing illumination, as expected. In all cases, the voltage was very uniform because the epitaxial GaAs solar cell has an extremely low density of recombination centers.[61] The very uniform colored scans shown in Figure 3b–i confirm the constant CPD signal of the cell, as expected for a GaAs monocrystalline device with extremely low density of defects (mostly from the original wafer used for the epitaxial growth of the device layers). Therefore, the uniform color of the scans means that the CPD does not vary within the resolution allowed by the AFM probe used (30 nm in diameter), rather than poor spatial resolution. Figure 3j shows the macroscopic V_{oc} (from solar simulator measurements) and the V_{oc} signal determined by KPFM, both as a function of the photon flux. For the KPFM measurements, the V_{oc} is the averaged signal obtained from the scans shown in Figure 3b–i. The calibration constant is $\beta = -0.73$ V (see Figure S2, Supporting Information). The KPFM measurements are in excellent agreement with the solar simulator ones: the ideality factor obtained from KPFM is $n = 1.9 \pm 0.2$, which is within 10% (see the Experimental Section). According to the KPFM measurements, the average V_{oc} of the solar cell at 1 sun illumination is $V_{oc} = 0.83 \pm 0.02$ V (spatially resolved in the inset of Figure 3j). These results demonstrate that by illuminated KPFM we can determine the macroscopic value of the V_{oc} for a device, as well as locally measure variations in V_{oc} with nanoscale resolution, which can be applied to nonuniform PV materials.

We extend the illuminated KPFM metrology to a variety of PV materials, allowing us to directly image local variations in V_{oc} (i.e., ΔV_{oc}) with nanoscale resolution. The ΔV_{oc} maps do not require system calibration, i.e., β is not needed. **Figure 4** shows the scanning electron microscopy (SEM), AFM, dark and illuminated KPFM measurements for all samples investigated in this work: GaAs, monocrystalline Si, CdTe, and CIGS, with morphologies ranging from epitaxial to granular surfaces. GaAs presents a very uniform V_{oc} (Figure 4q), with spatial variations within the noise level of the KPFM measurements (≈10 mV). The V_{oc} map for Si (Figure 4r) is also very uniform, as expected for a monocrystalline material. We investigate the influence of shadowing effects on the V_{oc} values for the textured Si sample—see Figure S5 (Supporting Information). Briefly, we find that to compensate the shadowing effects of the textured facets we simply need to measure illuminated KPFM under two illumination conditions. For CdTe (Figure 4s), different grain interfaces showed different V_{oc}, as indicated by the dashed areas. This result suggests that the grain boundaries act as distinct recombination centers. The CIGS grains present remarkable variations in V_{oc} (>200 mV), independent of the material topography, see dashed regions in Figure 4t. Despite the fact that the different facets of a crystal can present distinct work functions,[62] this difference is taken into account by our method because both the light and dark KPFM voltage signals are measured for the same facets of the crystal. The analysis of the role of the grain interfaces on the performance of the device is beyond the scope of this paper; however, our measurements demonstrate that nanoscale analysis of V_{oc} in nonuniform materials can resolve and quantify the recombination processes that currently limit the performance of polycrystalline solar cells.[63] Controlled growth of grains with crystal orientation corresponding to the high values of ΔV_{oc} (≈0.15 V) could potentially boost the overall V_{oc} of the device. Despite the fact that CIGS grains grow preferentially along the ⟨112⟩ orientation,[64] a distribution of grains is usually observed, and to the best of our knowledge there is no systematic study correlating different grain orientations with device performance. Note that while the voltage signal increases with illumination for GaAs, it decreases for Si and CdS/CIGS because the scanned layers are p- and n-doped, respectively. For the p-type CdTe surface,

© 2015 WILEY-VCH Verlag GmbH & Co. KGaA, Weinheim

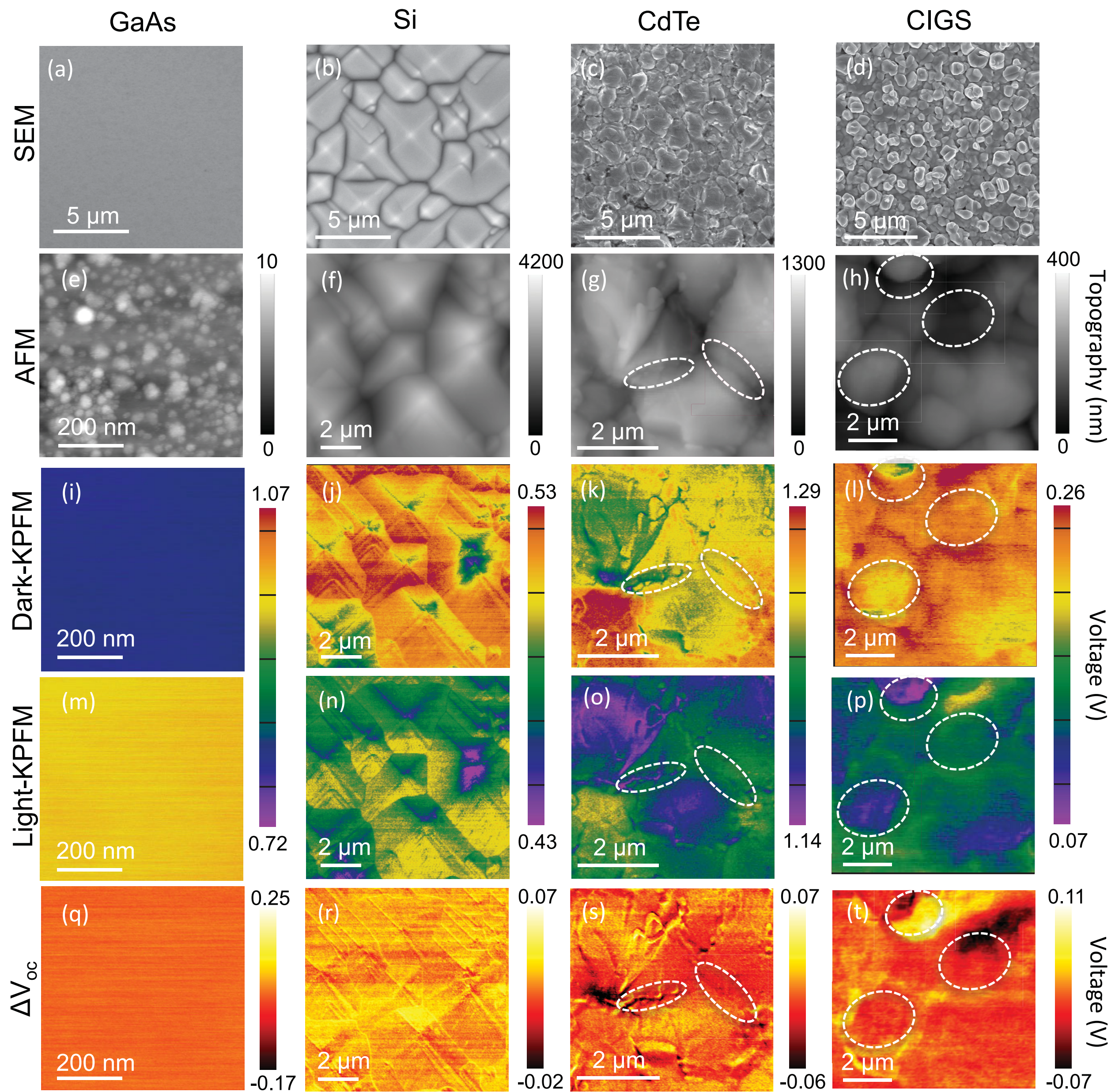

Figure 4. a–d) SEM images of GaAs, monocrystalline Si, CdTe, and CIGS solar cells. e–h) AFM topography images of the same samples. i–l) Dark KPFM images. m–p) Illuminated KPFM images using 660 nm laser source with power output = 1 mW, which corresponds to 1 sun illumination (100 mW cm^{-2}). For Si sample, laser output = 10 mW. q–t) Open-circuit voltage variation (ΔV_{oc}) maps with nanoscale resolution. Dashed areas indicate grains and interfaces with local V_{oc} variations only resolved by illuminated KPFM.

the voltage signal decreases with illumination because the work function of CdTe (≈5.9 eV) is larger than the work function of the Pt probe (≈5.1 eV) used in the measurements, modifying the band diagram configuration presented in Figure 1.

We resolve local variations in V_{oc} with spatial resolution <100 nm. **Figure 5**a shows a ΔV_{oc} map for the CdTe solar cell, with a few interfaces that have reduced V_{oc} and, most likely, act as nonradiative recombination centers. The full width half maximum (FWHM) of the line profiles shown in Figure 5b–d for the lateral variation in ΔV_{oc} is consistently below 100 nm. This set of KPFM measurements was acquired using Pt probes with 30 nm in diameter, demonstrating that we can accurately measure and resolve the V_{oc} with truly nanoscale resolution. Higher spatial resolution can be achieved by using smaller probes, such as high aspect ratio tips with gold nanoparticles on standard Si tips[65] or Si probes with 2 nm in diameter.[66]

For polycrystalline PV materials, the direct correlation between the structural properties of different grains and the V_{oc} maps can be used to identify the types of grains which should be favored during the thin-film deposition or growth. Further, nanostructured PV can tremendously benefit from this new technique because the identification of nonradiative recombination

© 2015 WILEY-VCH Verlag GmbH & Co. KGaA, Weinheim

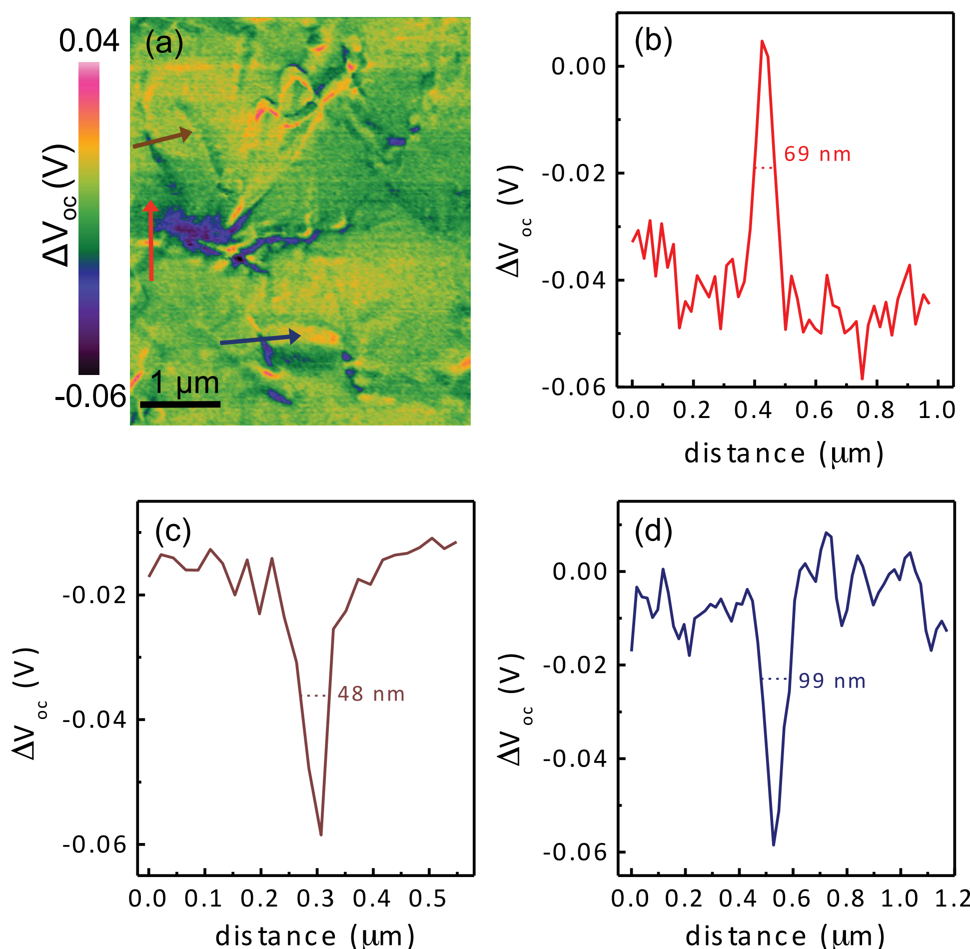

Figure 5. a) ΔV_{oc} map for CdTe solar cell. b–d) Line scans showing consistent spatial resolution <100 nm. The full width half maximum that defines the lateral resolution of the method is indicated in each line profile.

centers can guide the design of the next-generation nano-enabled devices. It is well known that the V_{oc} of a PV device can strongly depend on surface passivation, and therefore spatial variations in the surface properties can lead to local variations in the V_{oc}, which can be accurately measured with our technique. Further, a recombination center, which corresponds to a region with very small diffusion length, can be accurately measured by our imaging method. Although the carrier minority diffusion length of inorganic PV materials is greater than 100 nm, it is an average of the distance a carrier can move from point of generation until it recombines. Illuminated KPFM does not require the preceding knowledge of the sample nor the probe work function because the difference between the work function of the material surface and the probe under illumination and in the dark suffices to determine local variations in V_{oc}.

In summary, we present a new method to spatially resolve and image the V_{oc} in partially and fully processed optoelectronic devices with nanoscale resolution <100 nm. The V_{oc} is a key figure of merit to determine the performance of a device; it is an indirect measurement of the recombination processes that take place within the material. The illuminated KPFM technique is demonstrated in a variety of photovoltaic materials, ranging from epitaxial GaAs to polycrystalline CIGS, where we can resolve V_{oc} variation larger than 200 mV at the nanoscale. Our metrology, introduced here for the first time, can be applied to any optoelectronic device, including photovoltaics, light-emitting diodes (LEDs), and photodetectors, does not require full device processing, is nondestructive, and works in ambient environment. Moreover, it can be used to determine if specific device processing steps are beneficial or harmful for the ultimate performance of a functional semiconductor material.

Experimental Section

Solar Cells Fabrication: The GaAs solar cell was obtained from M-Comm, and the layer thicknesses are shown in Figure 2. The cells were grown on an n-type GaAs wafer (300 μm thick, 5×10^{18} cm^{-3}), and the active regions were cladded by AlGaAs (E_g = 1.80 eV, 3×10^{18} cm^{-3}) passivation and back surface field layers. The GaAs solar cell used for system calibration was extremely small (1×3 mm^2). As a consequence, the ideality factor of the device is particularly high, due to edge surface recombination effects.[67] The monocrystalline Si solar cell used was a commercially available device, formed by n- and p-doped Si layers, with pyramidal texturing to enhance light trapping. The commercially available CdTe solar cell measured was formed by the following layers (from top to bottom): 4.0 mm of glass substrate, 550 nm of a bilayer transparent conductive oxide, 50 nm of n-type CdS, and 3.5 μm of p-type CdTe, which

© 2015 WILEY-VCH Verlag GmbH & Co. KGaA, Weinheim

was submitted to the standard $CdCl_2$ treatment. Due to the geometry of the device, the illuminated KPFM measurements were performed on the exposed p-doped CdTe grains with the original back contact. The CIGS solar cell sample was fabricated by sputtering from a quaternary target, which consistently produces polycrystalline, highly oriented grains with controlled stoichiometry, and a band gap of 1.1 eV.[64] Soda lime glass coated with 700 nm of Mo was used as the substrate. p-doped CIGS films with 2.0 μm in thickness were deposited by RF magnetron sputtering. A 50 nm thick n-type CdS layer was deposited by chemical bath deposition. For all samples, no antireflection coating was added. Light *I–V* measurements for all the devices measured here are presented in Figure S7 (Supporting Information).

KPFM Measurements: The possible influence of major experimental artifacts was carefully analyzed, and no significant contribution to our measurements was found. A detailed study of the influence of ΔH (and therefore topography) on the SPV signal was performed and is presented in Figure S1 (Supporting Information). In order to minimize the effect of topography on the SPV signal, ΔH was kept constant for all dark and illuminated measurements presented here. Unless indicated otherwise, the probe passed at $\Delta H = 20$ nm above the topographic scan on the second pass. It has been shown that AM-KPFM is susceptible to internal AC-signal couplings which can lead to a topography-dependent offset in the applied voltage.[68] Thus, to ensure no topography pick up we measure the cantilever response to electrostatic excitation in both the in- and out-of-phase channels across the entire resonance. The response is that of a simple harmonic oscillator, without any sign of AC coupling. Because the coupling scales with frequency, we choose a cantilever with a low resonance frequency. Furthermore, the coupling is independent of illumination, so it does not affect our results pertaining to the change in surface potential caused by incident light intensity. The cantilever spatially averages the tip–sample interaction due to the long-range nature of the electrostatic interaction,[69] which does decrease the spatial voltage variation signal,[70] but does not change the voltage shift due to illumination.

Macroscopic Characterization of Devices: Dark and light *I–V* curves were acquired using a full spectrum solar simulator, with 2.0×2.0 in.^{2} (50.8×50.8 mm^2) collimated output, and an Air Mass 1.5G filter. The output power of the xenon lamp was independently controlled, ranging from 0.1 to 1.0 sun (100 mW cm^{-2}). The light source was calibrated using a 20×20 mm^2 reference monocrystalline Si solar cell with a fused silica window.

For the EQE measurements of GaAs, the light source used was a xenon arc lamp that was directed into a monochromator. Two identical silicon diodes were used to regulate the spectral response of the EQE measurements, one was used as a reference and the other for calibration. A beam splitter was placed to guide half of the output light to the fixed reference diode, the other half was directed through an optical path and collected at the position of the calibration diode or solar cell sample. The ratio of the spectral responses between the reference and calibration diode was computed in 10 nm increments. The EQE of the solar cell was determined between 390 and 900 nm. Independent calibrations were performed before each EQE measurement. A polarizer was used to match the polarization of the incident light with the illuminated KPFM measurements.

V_{oc} Image Analysis: The SPV images were corrected for drift using a correlation function which computes the similarity between two topographical scans as they shift in time. The function outputs a value that corresponds to the magnitude in which the image is shifted in *x* and *y*-directions. Once the topography correction was complete the potential maps of the dark and illuminated KPFM scans were subtracted.

Supporting Information

Supporting Information is available from the Wiley Online Library or from the author.

Acknowledgements

The authors acknowledge instrumentation assistance from D. Ha, D. Ma, J. Murray, B. Bartolo, T. Li, and Y. Zhang, and UMD Nanocenter, and financial support from the Clark School of Engineering at the University of Maryland. M.S.L. conceived and directed the research. E.M.T. and J.L.G. performed the KPFM measurements. E.M.T. performed macroscopic measurements and analyzed all the data presented in the paper. J.L.G. wrote the code to correct the drift of the images. J.A.F., J.D.M., R.Y.B., and J.S.S. designed and grew the CIGS samples. M.S.L. and J.N.M. analyzed the results. All authors commented on the paper. This project was funded through the Department of Materials Science and Engineering and the Institute for Research in Electronics and Applied Physics, at the University of Maryland. The authors declare no competing financial interest.

Received: June 9, 2015
Revised: July 23, 2015
Published online:

[1] P. K. Nayak, J. Bisquert, D. Cahen, *Adv. Mater.* **2011**, *23*, 2870.
[2] M. A. Green, K. Emery, Y. Hishikawa, W. Warta, E. D. Dunlop, *Prog. Photovoltaics* **2015**, *23*, 805.
[3] J. D. Major, R. E. Treharne, L. J. Phillips, K. Durose, *Nature* **2014**, *511*, 334.
[4] K. Catchpole, A. Polman, *Opt. Express* **2008**, *16*, 21793.
[5] P. Campbell, M. A. Green, *J. Appl. Phys.* **1987**, *62*, 243.
[6] J. N. Munday, H. A. Atwater, *Nano Lett.* **2010**, *11*, 2195.
[7] M. L. Brongersma, Y. Cui, S. Fan, *Nat. Mater.* **2014**, *13*, 451.
[8] M. D. McGehee, *Nat. Photonics* **2009**, *3*, 250.
[9] E. J. Spadafora, R. Demadrille, B. Ratier, B. Grévin, *Nano Lett.* **2010**, *10*, 3337.
[10] H. R. Moutinho, R. G. Dhere, C. S. Jiang, M. M. Al-Jassim, L. L. Kazmerski, *Thin Solid Films* **2006**, *514*, 150.
[11] I. Visoly-Fisher, S. R. Cohen, K. Gartsman, A. Ruzin, D. Cahen, *Adv. Funct. Mater.* **2006**, *16*, 649.
[12] K. Durose, S. E. Asher, W. Jaegermann, D. Levi, B. E. McCandless, W. Metzger, H. Moutinho, P. D. Paulson, C. L. Perkins, J. R. Sites, G. Teeter, M. Terheggen, *Prog. Photovoltaics* **2004**, *12*, 177.
[13] H. Sakaguchi, F. Iwata, A. Hirai, A. Sasaki, T. Nagamura, *Jpn. J. Appl. Phys.* **1999**, *38*, 3908.
[14] D. C. Coffey, O. G. Reid, D. B. Rodovsky, G. P. Bartholomew, D. S. Ginger, *Nano Lett.* **2007**, *7*, 738.
[15] C. Ballif, H. R. Moutinho, M. M. Al-Jassim, *J. Appl. Phys.* **2001**, *89*, 1418.
[16] M. J. Romero, C. S. Jiang, J. Abushama, H. R. Moutinho, M. M. Al-Jassim, R. Noufi, *Appl. Phys. Lett.* **2006**, *89*, 143120.
[17] H. R. Moutinho, R. G. Dhere, C. S. Jiang, T. Gessert, A. Duda, M. Young, W. K. Metzger, M. M. Al-Jassim, *J. Vac. Sci. Technol., B* **2007**, *25*, 361.
[18] J. S. Wilhelm Melitz, A. C. Kummel, S. Lee, *Surf. Sci. Rep.* **2011**, *66*, 1.
[19] P. Sutter, E. Sutter, T. R. Ohno, *Appl. Phys. Lett.* **2004**, *84*, 2100.
[20] P. Eyben, F. Seidel, T. Hantschel, A. Schulze, A. Lorenz, A. U. De Castro, D. Van Gestel, J. John, J. Horzel, W. Vandervorst, *Phys. Status Solidi A* **2011**, *208*, 596.
[21] O. G. Reid, H. Xin, S. A. Jenekhe, D. S. Ginger, *J. Appl. Phys.* **2010**, *108*, 084320.
[22] H. Hoppe, T. Glatzel, M. Niggemann, A. Hinsch, M. C. Lux-Steiner, N. S. Sariciftci, *Nano Lett.* **2005**, *5*, 269.
[23] S. Watanabe, Y. Fukuchi, M. Fukasawa, T. Sassa, A. Kimoto, Y. Tajima, M. Uchiyama, T. Yamashita, M. Matsumoto, T. Aoyama, *ACS Appl. Mater. Interfaces* **2014**, *6*, 1481.

© 2015 WILEY-VCH Verlag GmbH & Co. KGaA, Weinheim

[24] V. Palermo, G. Ridolfi, A. M. Talarico, L. Favaretto, G. Barbarella, N. Camaioni, P. Samorì, *Adv. Funct. Mater.* **2007**, *17*, 472.
[25] A. Soudi, C.-H. Hsu, Y. Gu, *Nano Lett.* **2012**, *12*, 5111.
[26] C.-S. Jiang, H. R. Moutinho, D. J. Friedman, J. F. Geisz, M. M. Al-Jassim, *J. Appl. Phys.* **2003**, *93*, 10035.
[27] C.-S. Jiang, D. J. Friedman, J. F. Geisz, H. R. Moutinho, M. J. Romero, M. M. Al-Jassim, *Appl. Phys. Lett.* **2003**, *83*, 1572.
[28] A. Schwarzman, E. Grunbaum, E. Strassburg, E. Lepkifker, A. Boag, Y. Rosenwaks, T. Glatzel, Z. Barkay, M. Mazzer, K. Barnham, *J. Appl. Phys.* **2005**, *98*, 084310.
[29] R. Baier, C. Leendertz, M. C. Lux-Steiner, S. Sadewasser, *Phys. Rev. B* **2012**, *85*, 165436.
[30] T. Dittrich, A. Gonzales, T. Rada, T. Rissom, E. Zillner, S. Sadewasser, M. Lux-Steiner, *Thin Solid Films* **2013**, *535*, 357.
[31] H. R. Moutinho, R. G. Dhere, C. S. Jiang, Y. F. Yan, D. S. Albin, M. M. Al-Jassim, *J. Appl. Phys.* **2010**, *108*, 074503.
[32] M. Hafemeister, S. Siebentritt, J. Albert, M. C. Lux-Steiner, S. Sadewasser, *Phys. Rev. Lett.* **2010**, *104*, 196602.
[33] M. Takihara, T. Minemoto, Y. Wakisaka, T. Takahashi, *Prog. Photovoltaics* **2013**, *21*, 595.
[34] S. S. Schmidt, D. Abou-Ras, S. Sadewasser, W. Yin, C. Feng, Y. Yan, *Phys. Rev. Lett.* **2012**, *109*, 095506.
[35] H. Mönig, Y. Smith, R. Caballero, C. A. Kaufmann, I. Lauermann, M. C. Lux-Steiner, S. Sadewasser, *Phys. Rev. Lett.* **2010**, *105*, 116802.
[36] M. S. Leite, M. Abashin, H. J. Lezec, A. G. Gianfrancesco, A. A. Talin, N. B. Zhitenev, *ACS Nano* **2014**, *8*, 11883.
[37] M. S. Leite, M. Abashin, H. J. Lezec, A. G. Gianfrancesco, A. A. Talin, N. B. Zhitenev, *IEEE J. Photovoltaics* **2014**, *4*, 311.
[38] M. K. Herndon, A. Gupta, V. Kaydanov, R. T. Collins, *Appl. Phys. Lett.* **1999**, *75*, 3503.
[39] A. A. McDaniel, J. W. P. Hsu, A. M. Gabor, *Appl. Phys. Lett.* **1997**, *70*, 3555.
[40] C. R. McNeill, H. Frohne, J. L. Holdsworth, J. E. Furst, B. V. King, P. C. Dastoor, *Nano Lett.* **2004**, *4*, 219.
[41] M. J. Romero, K. Alberi, I. T. Martin, K. M. Jones, D. L. Young, Y. Yan, C. Teplin, M. M. Al-Jassim, P. Stradins, H. M. Branz, *Appl. Phys. Lett.* **2010**, *97*, 092107.
[42] K. Bittkau, T. Beckers, *Phys. Status Solidi A* **2010**, *207*, 661.
[43] W. Bao, M. Melli, N. Caselli, F. Riboli, D. S. Wiersma, M. Staffaroni, H. Choo, D. F. Ogletree, S. Aloni, J. Bokor, S. Cabrini, F. Intonti, M. B. Salmeron, E. Yablonovitch, P. J. Schuck, A. Weber-Bargioni, *Science* **2012**, *338*, 1317.
[44] W. Bao, M. Staffaroni, J. Bokor, M. B. Salmeron, E. Yablonovitch, S. Cabrini, A. Weber-Bargioni, P. J. Schuck, *Opt. Express* **2013**, *21*, 8166.
[45] P. J. Schuck, A. Weber-Bargioni, P. D. Ashby, D. F. Ogletree, A. Schwartzberg, S. Cabrini, *Adv. Funct. Mater.* **2013**, *23*, 2539.
[46] K. Alberi, B. Fluegel, H. Moutinho, R. G. Dhere, J. V. Li, A. Mascarenhas, *Nat. Commun.* **2013**, *4*, 1.
[47] K. Bothe, G. H. Bauer, T. Unold, *Thin Solid Films* **2002**, *403*, 453.
[48] R. Berger, A. L. Domanski, S. A. L. Weber, *Eur. Polym. J.* **2013**, *49*, 1907.
[49] A. Castaldini, D. Cavalcoli, A. Cavallini, M. Rossi, *Mater. Sci. Eng., B* **2002**, *91*, 234.
[50] Q. Chen, H. Zhou, T.-B. Song, S. Luo, Z. Hong, H.-S. Duan, L. Dou, Y. Liu, Y. Yang, *Nano Lett.* **2014**, *14*, 4158.
[51] M. Chiesa, L. Bürgi, J.-S. Kim, R. Shikler, R. H. Friend, H. Sirringhaus, *Nano Lett.* **2005**, *5*, 559.
[52] J. Heo, S. Won, *Thin Solid Films* **2013**, *546*, 353.
[53] C. S. Jiang, H. R. Moutinho, R. G. Dhere, M. M. Al-Jassim, *IEEE J. Photovoltaics* **2013**, *3*, 1383.
[54] C.-S. Jiang, R. Noufi, K. Ramanathan, H. R. Moutinho, M. M. Al-Jassim, *J. Appl. Phys.* **2005**, *97*, 053701.
[55] M. Salvador, S. M. Vorpahl, H. Xin, W. Williamson, G. Shao, D. U. Karatay, H. W. Hillhouse, D. S. Ginger, *Nano Lett.* **2014**, *14*, 6926.
[56] G. Shao, M. S. Glaz, F. Ma, H. Ju, D. S. Ginger, *ACS Nano* **2014**, *8*, 10799.
[57] C. Yang, Y. Pyekh, S. Danyluk, *Sol. Energy Mater. Sol. Cells* **2012**, *102*, 167.
[58] L. Christian, Z. Ulrich, T. Sebastian, B. Elke, O. Tobias, G. Stefan, M. E. Lukas, *Nanotechnology* **2005**, *16*, S1.
[59] W. Bergbauer, T. Lutz, W. Frammelsberger, G. Benstetter, *Microelectron. Reliab.* **2006**, *46*, 1736.
[60] R. García, A. San Paulo, *Phys. Rev. B* **1999**, *60*, 4961.
[61] E. Y. Owen, D. Miller, S. R. Kurtz, *IEEE J. Photovoltaics* **2012**, *2*, 303.
[62] T. G. S. Sadewasser, *Kelvin Probe Force Microscopy: Measuring and Compensating Electrostatic Forces*, Springer - Verlag Berlin Heidelberg, **2011**.
[63] M. A. Green, K. Emery, Y. Hishikawa, W. Warta, E. D. Dunlop, *Prog. Photovoltaics* **2014**, *22*, 1.
[64] J. A. Frantz, R. Y. Bekele, V. Q. Nguyena, J. S. Sanghera, A. Bruce, S. V. Frolov, M. Cyrus, I. D. Aggarwal, *Thin Solid Films* **2011**, *519*, 7763.
[65] H. Silvia, P. Marcos, V. M. Cristina, L. Mónica, *Nanotechnology* **2013**, *24*, 395701.
[66] M. Cohen, R. Shavit, Z. Zalevsky, *Sci. Rep.* **2014**, *4*, 1.
[67] M. S. Carpenter, M. R. Melloch, M. S. Lundstrom, S. P. Tobin, *Appl. Phys. Lett.* **1988**, *52*, 2157.
[68] S. Barbet, M. Popoff, H. Diesinger, D. Deresmes, D. Theron, T. Melin, *J. Appl. Phys.* **2014**, *115*, 144313.
[69] H. O. Jacobs, P. Leuchtmann, O. J. Homan, A. Stemmer, *J. Appl. Phys.* **1998**, *84*, 1168.
[70] U. Zerweck, C. Loppacher, T. Otto, S. Grafström, L. M. Eng, *Phys. Rev. B* **2005**, *71*, 125424.

© 2015 WILEY-VCH Verlag GmbH & Co. KGaA, Weinheim